Magnetoelectric effect in functionalized few-layer graphene

Elton J. G. Santos

Phys. Rev. B **87**, 155440 — Published 30 April 2013

DOI: 10.1103/PhysRevB.87.155440

Magnetoelectric Effect in Functionalized Few-Layer Graphene

Elton J. G. Santos*
School of Engineering and Applied Sciences, Harvard University, Cambridge, Massachusetts 02138, USA

We show that the spin moment induced by sp^3-type defects created by different covalent functionalizations on a few-layer graphene structure can be controlled by an external electric field. Based on *ab initio* density functional calculations, including van der Waals interactions, we find that this effect has dependence on the number of stacked layers, concentration of point defects but the interplay of both with the electric field drives the system to a half-metallic state. The calculated magnetoelectric coefficient α has value comparable to those found for ferromagnetic thin films (e.g. Fe, Co, Ni) and magnetoelectric surfaces (e.g. CrO_2). The value of α also agrees with the universal value predicted for ferromagnetic half-metals and also points to a novel route to induce half-metallicity in graphene using surface decoration.

PACS numbers: 75.80.+q 75.70.Rf 75.75.-c 85.75.-d

I. INTRODUCTION

Magnetoelectric coupling has been attracting increasing interest as a way to lead to a new class of nanodevices. The possibility to manipulate the magnetization by an external electric field or the electrical polarization by an external magnetic field is of high fundamental and technological importance. Functional materials that presents such response to external fields are at the cutting edge of solid state research. Graphene is not an exception where the response to magnetic and electric fields has driven to the discovery of many fascinating effects. In particular, electric fields can change electronic transport[1], open band gaps[2], drive superconducting-insulating transition in hybrid system[3] and even control surface plasmons[4,5]. However, graphene is not magnetic which put limitations on its use in the context of magnetoelectric devices.

Here we address the issue of the magnetic moment induced by chemisorbed adsorbates in a few-layer graphene subjected to an external electric field. Some experiments have shown that the functionalization of graphene by H[6,7], F[8,9] and nitrophenyl diazonium molecules (NPD)[10–12] induce magnetic behavior. Through extensive *ab initio* electronic structure calculations, we show that the magnetic properties of covalently functionalized graphene can be manipulated by an external electric field. Functionalized monolayer (1L) graphene is not modified by the external field, while $N-$layer graphene ($N \geq 2$) displays a close dependence of the moment on the gate bias. The magnitude of the effect depends on the concentration of molecules and the sublattice adsorption site. Remaining, however, largely independent of the particular adsorbate considered which points to a *universal* behavior notwithstanding the functionalization used[13]. For example, the spin-electric response of NPD, COOH and NH_2 molecules are similar as that observed for H adatoms. This behavior is explained in terms of the band structure features and the interlayer charge-imbalance driven by the electric bias. The calculated magnetoelectric coefficient α has magnitude $\alpha = 5.74 - 10.43 \times 10^{-14}$ G cm^2/V, which is comparable to those found in ferromagnetic thin films and half-metallic surfaces. This indicates a robust electric response of the chemical modified graphene. A half-metallic character at low bias is also observed which is due to the capacitive depletion or accumulation of spin polarized carriers at the C surface. Our results point to a promising way to understand and controlling the interplay between electric fields and magnetism in functionalized graphene.

II. METHODS

The simulations reported here are based on density-functional-theory calculations using the SIESTA code.[14] The generalized gradient approximation[15] and nonlocal van der Waals density functional[16] was used together with double-ζ plus polarized basis set, norm-conserving Troullier-Martins pseudopotentials[17] and a mesh cutoff of 150 Ry. Atomic coordinates were allowed to relax using a conjugate-gradient algorithm until all forces were smaller than 0.04 eV/Å. Tests perform at better accuracy (<0.01 eV/Å) yields to almost identical relaxed structures. Relevant lattice constants (in-plane and out-of-plane) were optimized for each system taking into account the applied electric field. To avoid interactions between layer images, the distance between the graphene monolayers along the direction perpendicular to the C-atom plane was always larger than 20 Å. A $60 \times 60 \times 1$ k-sampling grid in the two-atom unit cell of graphene gives well converged values for all the calculated properties[18]. The fixed-spin method (FSM)[19,20] was also used to stabilize the magnetic solutions for some systems. The reason was that fluctuations on the value of the spin moment with the applied field were observed. We applied a spatially-periodic saw-tooth-like potential perpendicular to the graphene surface to simulate the external field across the supercell.

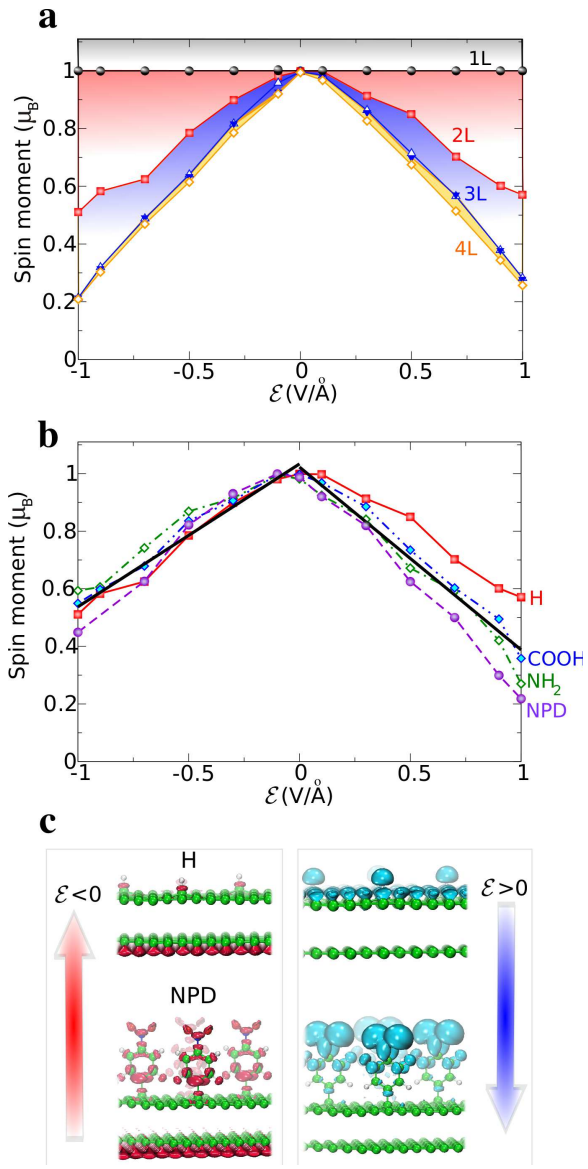

FIG. 1: **a,** Spin moment as a function of $\mathcal{E}$ for hydrogenated $N-$layer graphene. Both stacking orders were considered: ABA (N =2, 3, 4) and ABC (N =3) (filled triangles). **b,** Similar to **a,** but for other molecules chemisorbed on 2L graphene: NH_2, COOH, and NPD. The average of all curves is shown by the solid dark curve. **c,** Polarized charge density, $\Delta\rho = \rho(\mathcal{E}) - \rho(0)$, for functionalized 2L graphene with H (top panels) and NPD (bottom panels) molecules on the top layer. Left and right panels show $\Delta\rho$ at $\mathcal{E} < 0$ and $\mathcal{E} > 0$, respectively. Cutoff at $+0.004\ e^-/bohr^3$. The adsorbate concentration is 3.1%.

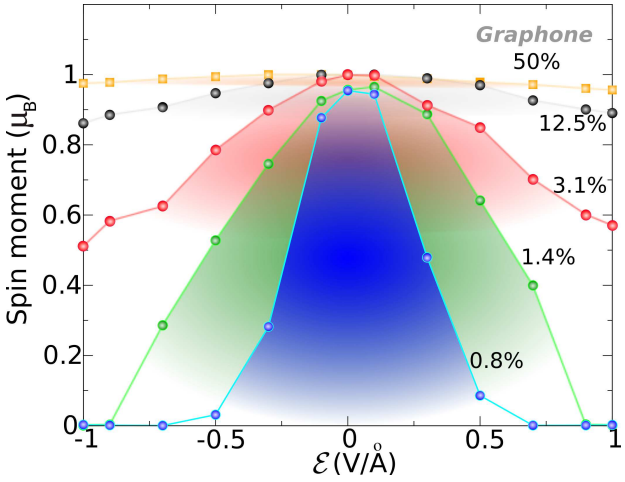

FIG. 2: Spin moment as a function of $\mathcal{E}$ for a hydrogenated 2L graphene at different concentrations. The molecular coverage varies from 50% (Graphone limit) to 0.8% (high-dilution limit considered).

III. MAGNETOELECTRIC RESPONSE

A. Universal Behavior

Figure 1**a,** shows the spin moment due to the hydrogenation of graphene as a function of the applied electric field $\mathcal{E}$. For 1L graphene the moment does not show any modification, remaining constant at its zero-field value of 1.0 μ_B per defect. 2L, 3L and 4L graphene display a clear dependence of the magnetic moment on $\mathcal{E}$ which in the studied range varies from 1.0 μ_B to 0.2 μ_B per defect. Our calculations also show that this effect is independent of the stacking order, Bernal (ABA) and Rhombohedral (ABC), giving numerically the same results for 3L graphene. Both stackings under an applied gate bias work in a different way as was recently reported[21–23] but the electric-spin dependence on the stacking of the graphene layers was not observed. The dependence of the spin moment on $\mathcal{E}$ saturates in 4L graphene with values close to that obtained for 3L graphene. Calculations performed for different chemisorbed adsorbates (NPD, NH_2, COOH) show similar results, which in principle is not an obvious behavior[13]. Figure 1**b** presents their dependence of the magnetic moment as a function of $\mathcal{E}$ on a 2L graphene. Despite of the particular adsorbate considered, the magnetic moment varies from 1.0 μ_B to 0.6/0.2 μ_B per defect side depending on the direction of the applied field. An increasing asymmetry on the damping of the spin moment is observed from H to NPD molecules at positive external fields. This is due to the polarized charge density $\Delta\rho$ induced on the adsorbates as shown in Figure 1**c**. For H adatoms at $\mathcal{E} > 0$, $\Delta\rho$ has contribution from both the C-surface and the adsorbate (upper right panel in Fig. 1**c**). However, for NPD $\Delta\rho$ is mainly localized at the molecule on the NO_2 radical which is more polarizable under the field (lower right panel in Fig. 1**c**). This generates an additional charge density that helps to dampen the magnetic moment to lower values.

B. Molecular Coverage and Disorder

We address next the dependence of the magnetoelectric effect on the molecular coverage. In Figure 2 we plot the spin moment as a function of the field $\mathcal{E}$ for a 2L graphene at 50%, 12.5%, 3.1%, 1.4% and 0.8% coverage. At the limit of Graphone (50%), where half-side of graphene is fully functionalized, the magnetic moment does not change significantly. It keeps its value of 1.0 μ_B at $\mathcal{E} = 0$. As the coverage is reduced the variation of the magnetic moment with the field becomes stronger. At the dilute limit considered here, ∼0.8%, variations of 100% in the value of the magnetic moment are obtained for $\mathcal{E}$ =0.5 V/Å. This suggests that for a hydrogenated few-layer graphene at high dilution ($< 28.9\ 10^{12}/\mathrm{cm}^2$), an external field can induce switching between ON and OFF states similar to that in magnetoresistance[24] and magnetoelectric devices[25]. This is in close agreement with recent SQUID measurements, performed for defective and functionalized multilayer graphene where the interplay between magnetism and electrical means was detected[26].

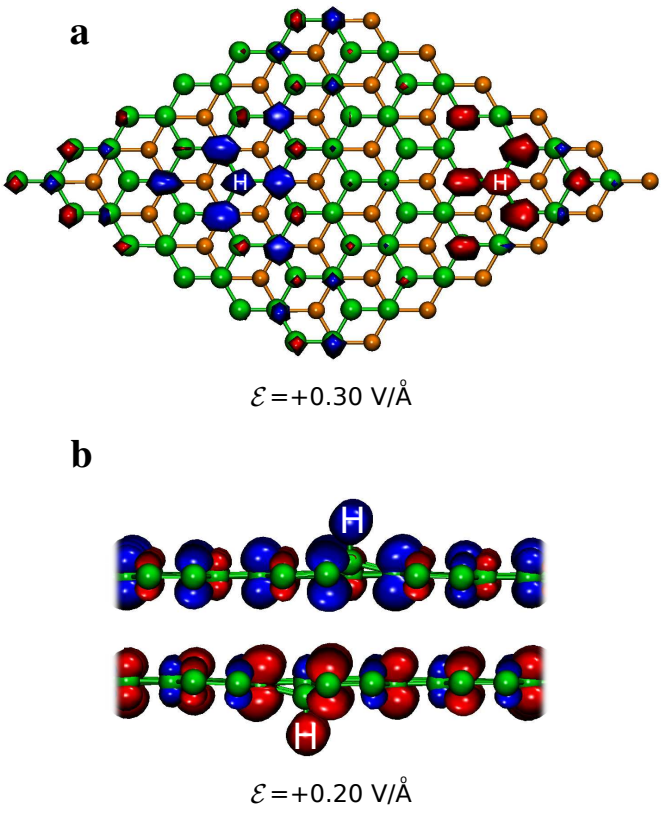

FIG. 3: (Color online) Spin magnetization density for 2L graphene with H adatoms at different sublattices: **a,** at the same layer (A^1B^1) and **b,** at different layers (A^1B^2). Spin up and spin down are defined for positive (dark blue) and negative (light red) isosurfaces. The value of the external field $\mathcal{E}$ is given in each panel. Cutoffs at $\pm 0.007\ e^-/bohr^3$ and $\pm 0.01\ e^-/bohr^3$ in **a,** and **b,** respectively. The bottom layer in **a,** has a different color in comparison to the top one.

Possible effects of disorder and functionalization at different layers were also studied. We considered H atoms as the test molecule, because of its high reactivity with C and its small steric size compared to the other adsorbates, may help the diffusion to other layers. Bigger molecules, in particular NPD, were not considered due to their periodic coverage recently observed[10–12]. For two H atoms at the same layer, but at different sublattices (A^1B^1), $\mathcal{E}$ generates a spin moment of ∼0.10 μ_B (see Figure 3**a**). It comprises the first impurity neighbors with an antiferromagnetic (AFM) spin coupling between them. The calculated exchange energy ($J_{A^1B^1}$) gives $J_{A^1B^1}$ ∼2 meV which also depends on the relative distribution of H atoms. An electric-spin response is observed as long as the impurities do not cluster or form dimmers[27]. Simulations carried out for many H positions confirm this trend. When hydrogenation takes place at different layers[28] but at the same sublattice (A^1A^2), both ferromagnetic (FM) and AFM solutions are energetically stable with $J_{A^1A^2}$ ∼2.1 meV. The total spin magnetization integrates to 2.00 μ_B in the FM case, at zero field, with a similar tuning of the magnetic properties as that in A^1A^1 situation. If the two molecules are located at different sublattices (A^1B^2) the AFM configuration is the most stable[29]. The energy difference in relation to the spin compensated solutions, closer in energy than the FM ones, is $E_{A^1B^2}$ =31 meV/cell at $\mathcal{E}$ =0. For this configuration an AFM-magnetoelectric response is observed as displayed in Figure 3**b**.

IV. MAGNETOELECTRIC COEFFICIENTS AND HALF-METALLIC BEHAVIOR

A. Fitting

Next we calculate the magnetoelectric coefficient α_{ij} which quantifies the interplay between the magnetization M and electric fields. This is given by the tensor $\alpha_{ij} = \mu_0 \left(\frac{\partial M_i}{\partial \mathcal{E}_j}\right)$, where μ_0 is the vacuum magnetic permeability constant. In this approximation only the transverse component, $\alpha_{zz} = \alpha^{\mathcal{E}}$, will be considered. Because the orbital contribution L to the magnetization $M = S + L$, which determines the other components (α_{xx}, α_{yy}, α_{xy}, etc.), is small in carbon. Fitting the data shown in Figure 1**b** to $\alpha^{\mathcal{E}}$ we find $\alpha^{\mathcal{E}}$ in the range of $-10.43 - +7.72\ 10^{-14}$ G cm^2/V as shown in Table I for each adsorbate and field polarization. The different signs of $\alpha^{\mathcal{E}}$ is due to the different orientation of the magnetic moment at the defect side under $\mathcal{E}$. The calculated values of $\alpha^{\mathcal{E}}$ are $\sim 3-6$ times larger than those in ferromagnetic metal films (Fe(001), Co(0001), Ni(001))[30] but smaller in comparison with interfaces based on perovskites ($SrRuO_3/SrTiO_3$)[31]. Both types of systems contain heavy metal atoms (with $3d$ or $4d$ electrons), in contrast with functionalized graphene which contains only light C and H atoms ($2s$ and $2p$ electrons). The average

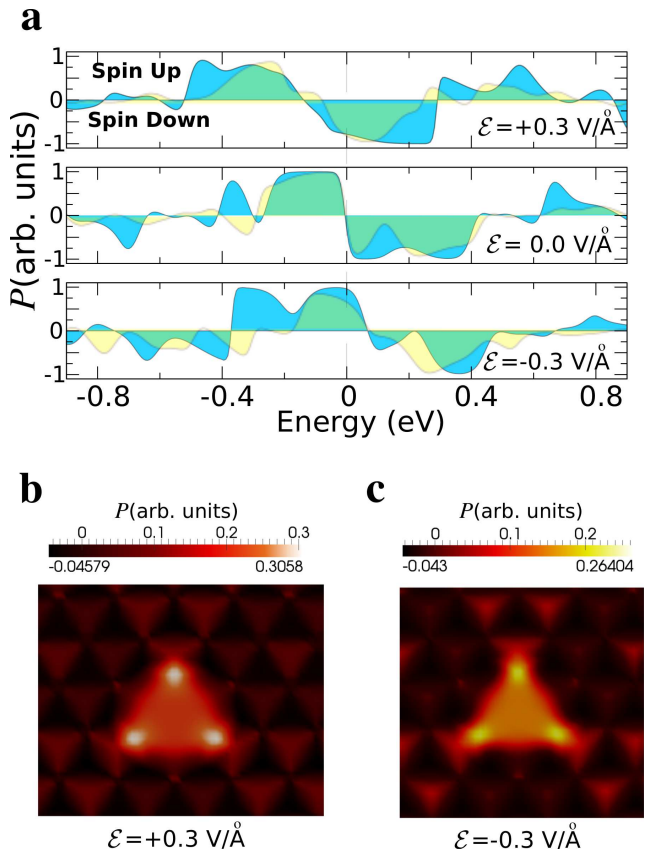

FIG. 4: **a,** Spin polarization P of hydrogenated 2L (blue curve) and 3L (faint yellow curve) graphene at $\mathcal{E}$ =+0.3 V/Å, 0.0 V/Å and -0.3 V/Å. Positive and negative values of P correspond to up and down spins. E_F is marked by the dashed vertical line. **b,** and **c,** show the respective cross section of P ($\pm 0.02\ e^-/bohr^2$) at $\mathcal{E}$ =+0.3 V/Å and -0.3 V/Å. The color gradient represents the relative polarization of the C atoms for up and down spins.

calculated values of $\alpha^{\mathcal{E}<0} = +6.68$ and $\alpha^{\mathcal{E}>0} = -8.54$ are close to the universal value $\alpha_U = 6.44 \times 10^{-14}$ G cm^2/V for ferromagnetic half-metallic surfaces (CrO_2 (001))[32].

TABLE I: Calculated magnetoelectric coefficients ($\alpha^{\mathcal{E}}$) in a functionalized 2L graphene at positive and negative external electric fields.

Adsorbates	H	NH_2	COOH	NPD
$\alpha^{\mathcal{E}<0}$ (10^{-14} G cm^2/V)	6.84	5.74	6.41	7.72
$\alpha^{\mathcal{E}>0}$ (10^{-14} G cm^2/V)	-6.20	-9.08	-8.54	-10.43

B. Electrical Spin-Filtering Effect

We note that functionalized graphene multilayers exhibit half-metallic behavior. This is shown in Figure 4**a,** by the behavior of the polarization P for bilayer 2L and trilayer 3L graphene as a function of the energy. P is defined by $P = \frac{N_\uparrow(E)-N_\downarrow(E)}{N_\uparrow(E)+N_\downarrow(E)}$, where $N_\sigma(E)$ is the spin-dependent ($\sigma =\uparrow$ or $\downarrow$) density of states. At $\mathcal{E} = \pm 0.30$ V/Å , in both graphene stackings, just one spin channel (up or down) appears around the Fermi level (E_F) leading to almost complete polarization, $|P| \approx 1$. The main atoms that contribute to this effect are localized at the first C-neighbors to the defect side as is shown in Figure 4**b**,**c** at distinct field polarization. This means that covalent functionalization can create *patches* of spins at specific state, driven by the electric field, which can efficiently work as a spin-filter. Our simulations also point that the magnetic interaction energies are large. The energy difference between the half-metallic state at $\mathcal{E} = \pm 0.30$ V/Å and $\mathcal{E} = 0$ V/Å is 8 meV per carbon atom. This value should be compared to the spin-polarized edge state of graphene nanoribbons, which has a polarization energy of ∼20 meV per edge atom[33]. We note that the creation of graphene nanoribbons with well controlled edges is probably more difficult than the creation of covalently functionalized graphene samples[10–12].

V. INTERLAYER CHARGE IMBALANCE

A. Electrically-Driven Spin State

We now analyze the origin of this half-metallicity as well as the magnetoelectric effect. Figure 5**a,b,d,e,** show the electronic structure of functionalized 1L and 2L graphene system. The results are for H adatoms but they are equivalent to the other adsorbates as commented above. In 1L graphene (Fig. 5**a**), the adsorbate introduces a very narrow defect state that is pinned at E_F. This state shows a predominant $2p_z$ contribution from the nearest C-neighbors of the defect site, with a smaller component from the adsorbate itself as seen in Fig. 5**c**. The small dispersion of this $2p_z$-defect band combined with its partially filled character favors the spin-uncompensated solutions. The splitting energy between up and down $2p_z$-defect bands gives ∼0.30 eV at the Γ point, inside of a gap of ∼1.3 eV between C-states from the graphene surface. The behavior is similar for 2L graphene, except that the presence of the second pristine C layer reduces this gap to zero, and the interaction of the bands at the K point produces some dispersion in the two defect states (see Figure 5**b**). The second pristine C layer introduces a Dirac cone at K in the functionalized system that at $\mathcal{E} = 0$ is still at the neutrality point.

The application of an electric bias on the 1L graphene produces no change in its band structure (see Figure 6), but induces a pronounced effect in the band structure of

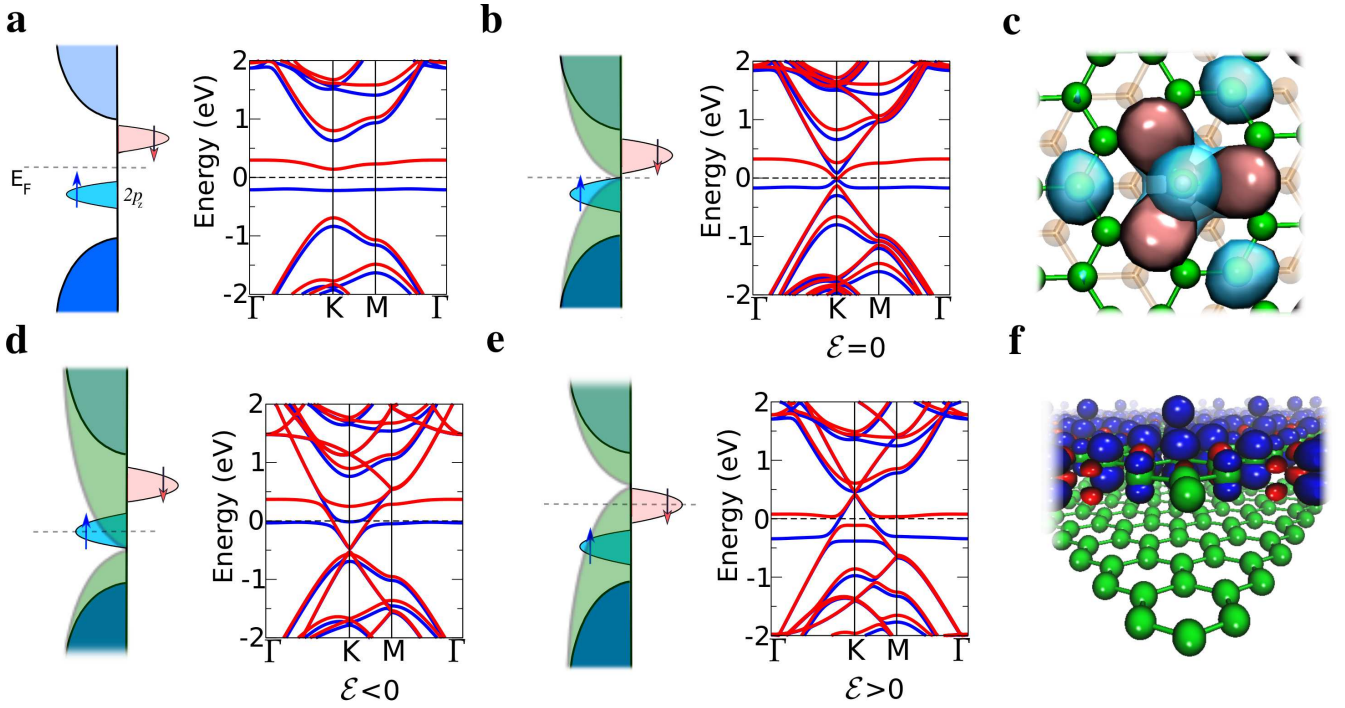

FIG. 5: Schematic representation of the electronic structure (on left) and calculated band structure (on right) of hydrogenated graphene for: **a,** 1L and **b,** 2L graphene both at $\mathcal{E} = 0$; spin up and spin down states are shown in blue (dark) and red (bright) lines. The dashed line shows E_F for each electronic structure. **c,** Wavefunction of the defect state in 2L graphene (± 0.04 $e^-/bohr^3$) at the Γ point and $\mathcal{E} = 0$; positive and negative values are shown in light pink and cyan surfaces. The bottom layer is shown in light orange color. **d,** and **e**, are the corresponding band structures for the 2L graphene, at $\mathcal{E} = -0.50$ V/Å and $+0.50$ V/Å. **f,** Magnetization density (± 0.02 $e^-/bohr^3$) at $\mathcal{E} = 0$ for 2L graphene. The adsorbate concentration is 3.1%.

the 2L graphene. In particular, the electric field shifts the Dirac cone of the pristine layer relative to the position of the defect bands. This shift induces an interlayer charge-transfer which depends on the field polarization. Figure 5**d**,**e**, show these effects for $\mathcal{E} = -0.50$ V/Å and $+0.50$ V/Å, respectively, with the defect states shifting to higher and lower energy (∼0.33 eV). This corresponds to the observed half-metallic state. Increasing $\mathcal{E}$ leads to gradual occupation of the opposite spin state and the corresponding damping of the spin moment and polarization P discussed earlier.

B. Electrical Capacitance and its Spin Analogous

The effect of the induced charge transfer Δn between the pure and hydrogenated layers in functionalized 2L graphene is shown in Figure 7. We found that Δn increases or decreases approximately linear with the field (solid black line), which is a behavior expected from a parallel plate capacitor[2]. This results in a charge capacitance per unit area $C = \Delta n/\Delta V$, with $\Delta V = d\ (\mathcal{E}/\varepsilon)$ where d is the distance between the capacitor plates and ε is the effective dielectric constant between the plates. We calculate ε by comparing the average electric field in the region between the two C-planes and taking the ratio to the externally applied field: $\varepsilon = \mathcal{E}_{\rm ext}/\mathcal{E}_{\rm eff}$.

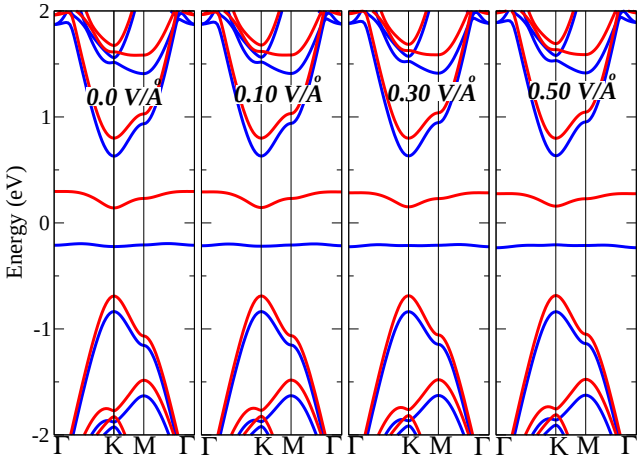

FIG. 6: (Color online) Spin polarized band structures for hydrogenated 1L graphene at 3.1% coverage. From the left to the right panel, the electric fields are +0.0, +0.10, +0.30, +0.50 V/Å, respectively. Up and downs spins are shown in blue and red colors, respectively. E_F is set to zero in all panels.

We obtain $\varepsilon \sim 2 - 4$ which agrees well with recent scanning tunneling microscopy[34] and magnetoresistance measurements[35]. We use the value $\varepsilon = 3$ which is in the

middle of the range. However, it is worth noting that ε is electric-field dependent as recently shown[36]. For 2L graphene the modifications are smaller than ∼4% which allows us to use the same value of ε in the calculated range of fields. The values of the capacitance of the pristine C_0 and functionalized systems C_H give $C_0 \approx 5.7$ μF cm^{-2} and $C_H \approx 6.9$ μF cm^{-2}. The capacitance of the pristine system C_0 is also in close agreement with recent experiments[35] which report values in the range 6.8–7.5 μF cm^{-2}. It is important to compare the capacitance calculated here to values predicted for $SrRuO_3/SrTiO_3$ interfaces[31], of 2.0 μF cm^{-2}, which shows that they are in the same magnitude.

The spin capacitance C^S is another quantity of interest in systems that exhibit spin-polarization and can be relevant to the performance of spintronic devices based on functionalized graphene materials. It is defined by[31] $C^S = \Delta\xi/\Delta V$, where $\Delta\xi$ is the amount of spin-polarized charge density per unit area induced by the voltage difference ΔV. In our systems, where charge mediates spin compensation, we expect that $C^S_H = C_H$ should be validated. We have verified numerically that this relation holds to an accuracy better than 1%. Therefore, in functionalized 2L graphene C^S_H is of the same order of magnitude as that found for $SrRuO_3/SrTiO_3$ structures[31].

VI. ELECTROSTATIC EXFOLIATION

We have also observed that there exist a limit on the intensity of the external field that can be applied to the functionalized multilayer graphene. Figure 8 shows the total energy for hydrogenated bilayer graphene as a function of the interlayer distance z. The equilibrium distance (z_{eq}) is 3.4 Å. At $\mathcal{E}$ =0.0 V/Å, a van der Waals barrier (ΔE_{vdW}) of ΔE_{vdW} =28.50 meV/atom prevents the separation of the two layers from z_{eq} to infinity. For $\mathcal{E} \neq 0$ the value of ΔE_{vdW} decreases, pointing that the C-planes become weaker bound. At $\mathcal{E}$ =1.88 V/Å, the two planes of the functionalized 2L graphene can be easily separated with $\Delta E_{vdW} \sim 1.0$ meV/atom. This effect is due to the electrostatic attraction force acting between the graphene surface and the bias gate which compensates the van der Waals forces between the layers. Similar observations were experimentally used to exfoliate highly oriented pyrolytic graphite in prepatterned few-layer graphene using an electrostatic gate[37]. Thus, the intensity of the external field should be carefully controlled in order to just change the value of the magnetic properties of the functionalized graphene structure, without inducing to exfoliation.

VII. CONCLUSIONS

In conclusion, we have used first-principles electronic structure calculations to demonstrate the interplay between electric and magnetic properties in functionalized few-layer graphene. The electrical-spin response is comparable to that observed in systems where heavy elements play a role. This provides an additional degree of freedom in the design and modification of graphene-based materials, opening new possibilities in spintronics and magnetoelectric devices.

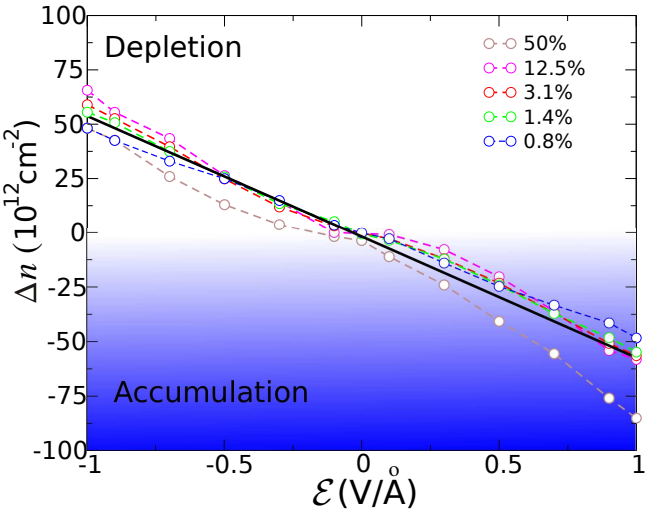

FIG. 7: Charge transfer density Δn as a function of $\mathcal{E}$ for 2L graphene at different H coverage. The average of all curves is shown by the solid dark curve. The accumulation and depletion regions are highlighted.

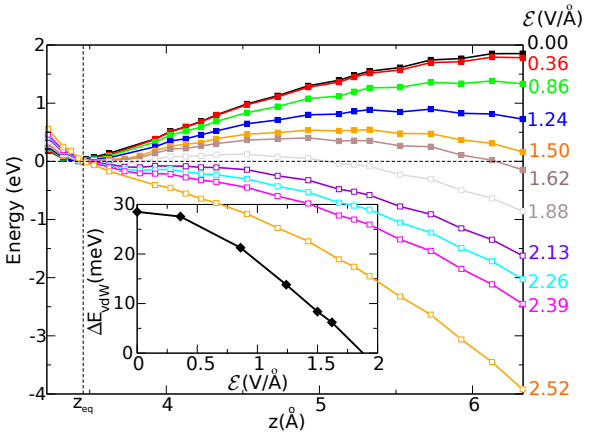

FIG. 8: Total energy versus interlayer distance for hydrogenated bilayer graphene at different values of $\mathcal{E}$(V/Å). The vertical dashed line indicates the equilibrium position z_{eq}. The inset shows the van der Waals barrier (ΔE_{vdW}) per atom as a function of $\mathcal{E}$. The adsorbate coverage is at 3.1%.

VIII. ACKNOWLEDGMENTS

We thank David Goldhaber-Gordon, Robert C. Haddon, Sakhrat Khizroev, F. Guinea and Antonio H. Castro Neto for valuable discussions. We have used the

Extreme Science and Engineering Discovery Environment (XSEDE), supported by NSF grant numbers TG-DMR120049, TG-DMR120073 and TG-PHY120021.

* Electronic address: esantos@seas.harvard.edu

[1] S. Das Sarma, S. Adam, E.H. Hwang, and E. Rossi, Rev. Mod. Phys. **83**, 407 (2011).

[2] E. V. Castro, K. S. Novoselov, S. V. Morozov, N. M. R. Peres, J. M. B. Lopes dos Santos, J. Nilsson, F. Guinea, A. K. Geim and A. H. Castro Neto, Phys. Rev. Lett. **99**, 216802 (2007).

[3] A. Allain, Z. Han and V. Bouchiat, Nat. Materials **11**, 590 (2012).

[4] J. Chen, M. Badioli, P. Alonso-Gonzalez, S. Thongrattanasiri, F. Huth, J. Osmond, M. Spasenovic, A. Centeno, A. Pesquera, P. Godignon, A. Zurutuza-Elorza, N. Camara, F. J. G. de Abajo, R. Hillenbrand, F. H. L. Koppens, Nature **487**, 77 (2012).

[5] Z. Fei, A. S. Rodin, G. O. Andreev, W. Bao, A. S. McLeod, M. Wagner, L. M. Zhang, Z. Zhao, M. Thiemens, G. Dominguez, M. M. Fogler, A. H. C. Neto, C. N. Lau, F. Keilmann, D. N. Basov, Nature **487**, 82 (2012).

[6] L. Xie, X. Wang, J. Lu, Z. Ni, Z. Luo, M. Mao, R. Wang, Y. Wangand, H. Huang, D. Qi, R. Liu, T. Yu, Z. Shen, T. Wu, H. Peng, B. Ozyilmaz, K. Loh, A. T. S. Wee, Ariando, W. Chen, Appl. Phys. Lett. **98**, 193113 (2011).

[7] K. M. McCreary, A. G. Swartz, W. Han, J. Fabian and R. K. Kawakami, Phys. Rev. Lett. **109**, 186604 (2012).

[8] X. Hong, K. Zou, B. Wang, S.-H. Cheng and J. Zhu, Phys. Rev. Lett. **108**, 226602 (2012).

[9] R. R. Nair, M. Sepioni, I. L. Tsai, O. Lehtinen, J. Keinonen, A. V. Krasheninnikov, T. Thomson, A. K. Geim, I. V. Grigorieva, Nat. Physics **8**, 199 (2012).

[10] J. Hong, E. Bekyarova, P. Liang, W. A. de Heer, R. C. Haddon and S. Khizroev, Sci. Rep. **2:624**, (2012). DOI: 10.1038/srep00624.

[11] J. Hong, S. Niyogi, E. Bekyarova, M. E. Itkis, P. Ramesh, N. Amos, D. Litvinov, C. Berger, W. A. de Heer, S. Khizroev, R. C. Haddon, Small **7**, 1175 (2011).

[12] S. Niyogi, E. Bekyarova, J. Hong, S. Khizroev, C. Berger, W. de Heer, R. C. Haddon, The Journal of Physical Chemistry Letters **2**, 2487 (2011).

[13] E. J. G. Santos, A. Ayuela, A. and D. Sánchez-Portal, New Journal of Physics **14**, 043022 (2012).

[14] J. M. Soler, E. Artacho, J. D. Gale, A. Garcia, J. Junquera, P. Ordejon, D. Sánchez-Portal, *J. Physics: Condensed Matter* 2002, **14**, 2745.

[15] J. P. Perdew, K. Burke, M. Ernzerhof, *Phys. Rev. Lett.* 1996, **77**, 3865.

[16] M. Dion, H. Rydberg, E. Schröder, D. C. Langreth, B. I. Lundqvist, *Phys. Rev. Lett.* 2004, **92**, 246401.

[17] N. Troullier, J. L. Martins *Phys. Rev. B* 1991, **43**, 1993.

[18] H. J. Monkhosrt, J. D. Pack, *Phys. Rev. B* 1976, **13**, 5188.

[19] A. R. Williams, V. L. Moruzzi, J. Kübler, K. Schwarz, *Bull. Am. Phys. Soc.* 1984, **29**, 278.

[20] T. Jarlborg, A. J. Freeman, *Phys. Rev. B* 1981, **23**, 3577.

[21] C. H. Lui, L. Zhiqiang, K. F. Mak, E. Cappelluti and T. F. Heinz, Nat. Physics **7**, 944 (2011).

[22] W. Bao, L. Jing, J. Velasco, Y. Lee, G. Liu, D. Tran, B. Standley, M. Aykol, S. B. Cronin, D. Smirnov, M. Koshino, E. McCann, M. Bockrath, C. N. Lau, Nat. Physics **7**, 948 (2011).

[23] L. Zhang, Y. Zhang, J. Camacho, M. Khodas and I. Zaliznyak, Nat. Physics **7**, 953 (2011).

[24] D. Soriano, N. Leconte, P. Ordejón, J. C. Charlier, J. J. Palacios and S. Roche, Phys. Rev. Lett. **107**, 016602 (2011).

[25] M. Fiebig, J. Phys. D: Appl. Phys. **38**, 123 (2005).

[26] R. R. Nair, I. L. Tsai, M. Sepioni, O. Lehtinen, J. Keinonen, A. V. Krasheninnikov, A. H. Castro Neto, A. K. Geim, I. V. Grigorieva, *arXiv:1301.7611.*

[27] R. Balog, B. Jorgensen, L. Nilsson, M. Andersen, E. Rienks, M. Bianchi, M. Fanetti, E. Laegsgaard, A. Baraldi, S. Lizzit, Z. Sljivancanin, F. Besenbacher, B. Hammer, T. G. Pedersen, P. Hofmann, L. Hornekaer, Nat. Materials **9**, 315 (2010).

[28] We considered the hydrogenation at the external side of graphene surfaces. Calculations performed with H atoms at the internal side of the layers resulted to be energetically higher in energy than those at the external one: 138 meV and 77 meV at A^1A^2 and A^1B^2 configurations, respectively.

[29] The total energy of A^1A^2 hydrogenation is higher than the A^1B^2 one by 93 meV per cell, at $\mathcal{E}$ =0, and increases with the gate bias.

[30] C. G. Duan, J. P. Velev, R. F. Sabirianov, Z. Zhu, J. Chu, S. S. Jaswal and E. Y. Tsymbal, Phys. Rev. Lett. **101**, 137201 (2008).

[31] J. M. Rondinelli, M. Stengel and N. A. Spaldin, Nat. Nanotechnology **3**, 46 (2008).

[32] C. G. Duan and C. W. Nan and S. S. Jaswal and E. Y. Tsymbal, Phys. Rev. B(R) **79**, 140403 (2009).

[33] Y. W. Son, M. L. Cohen and S. G. Louie, Nature **444**, 347 (2006).

[34] Y. Wang, V. W. Brar, A. V. Shytov, Q. Wu, W. Regan, H. Z. Tsai, A. Zettl, L. S. Levitov, M. F. Crommie, Nature Phys. **8**, 653 (2012).

[35] J. D. Sanchez-Yamagishi, T. Taychatanapat, K. Watanabe, T. Taniguchi, A. Yacoby and P. Jarillo-Herrero, Phys. Rev. Lett. **108**, 076601 (2012).

[36] E. J. G. Santos, and E. Kaxiras, *Nano Letters* **13**, 898 (2013).

[37] X. Liang, A. S. P. Chang, Y. Zhang, B. D. Harteneck, H. Choo, D. L. Olynick, S. Cabrini, Nano Letters **9**, 467-472 (2009).